

Aerodynamic Drag Reduction for Ground Vehicles using Lateral Guide Vanes

E.M. Wahba^C, H. Al-Marzooqi, M. Shaath, M. Shahin, T. El-Dhmashawy

*Mechanical Engineering Department, College of Engineering
American University of Sharjah, UNITED ARAB EMIRATES*

Received: 11/02/2012 – Revised 07/04/2012 – Accepted 13/04/2012

Abstract

The use of lateral guide vanes as a drag reducing device for ground vehicles is numerically investigated in the present study using computational fluid dynamics. Two types of ground vehicles are considered, a simplified bus model and a simplified sport utility vehicle (SUV) model. The guide vanes are used to direct air into the low-pressure wake region in order to enhance pressure recovery, which in turn would reduce form drag and hence the overall aerodynamic drag. The steady-state simulations are based on the Reynolds-averaged Navier-Stokes equations, with turbulence closure provided through two-equation eddy-viscosity models. Guide vane cross-section, chord length and angle of attack are varied in order to obtain the optimal configuration for improved aerodynamic performance. Simulations indicate an overall reduction in the aerodynamic drag coefficient of up to 18% for the bus and SUV models with the use of the lateral guide vanes. Moreover, it is shown that guide vanes with symmetric airfoil cross-sections result in higher percentage drag reduction as compared to asymmetric cross-sections. Grid-independence tests and comparison with available data in the literature is carried out to validate the present numerical procedure.

Keywords: Drag reduction; vehicle aerodynamics; turbulence modelling; form drag; Reynolds Averaged Navier-Stokes equations.

1. Introduction

Sport utility vehicles, trucks, vans and buses are examples of large ground vehicles that are often criticized for their poor fuel economy. With recent spikes in fuel prices and a worldwide trend towards controlling greenhouse gas emissions, automotive design engineers are faced with the immediate task of introducing more efficient aerodynamic designs for such vehicles.

In general, such vehicles are known to be aerodynamically inefficient compared to other ground vehicles due to their large frontal areas and bluff-body shapes. The inefficient aerodynamic shape results in excessive drag which leads to elevated fuel consumption rates. Contributions to heavy vehicle aerodynamic drag are mainly due to pressure drag, also known as form drag. It is

^C Corresponding Author: E.M. Wahba

Email: emwahba@yahoo.com

© 2009-2012 All rights reserved. ISSR Journals

PII: S2180-1363(12)4268-X

estimated that the pressure drag on heavy vehicles accounts to more than 80% of the total aerodynamic drag [1], with frictional drag accounting for the remaining 20%.

Computational fluid dynamics provides a valuable tool for the analysis of heavy vehicle aerodynamics. Numerical studies aimed at evaluating the use of computational fluid dynamics for the prediction of the overall drag coefficient for heavy vehicles have been carried out by a number of researchers [2–4]. Salari et al. [2] used Reynolds-averaged Navier-Stokes (RANS) simulations together with experimental data for a simplified tractor/trailer geometry to show that with an appropriate choice of turbulence model, the overall drag coefficient could be predicted with reasonable accuracy. Pointer [3] used a commercial CFD flow solver to study a realistic tractor-trailer combination, and the results indicated that the overall drag coefficient could be predicted with reasonable accuracy. Maddox et al. [4] used another commercial CFD solver to simulate the flow around a simplified tractor/trailer geometry. They employed a detached eddy simulation (DES) approach and showed that an improvement in the predicted pressure (especially toward the base of the model) can be achieved. Large eddy simulations (LES) of road vehicle aerodynamics were carried out by Verzicco et al [5], where the predicted averaged drag coefficient and mean velocity profiles were in good agreement with experimental measurements.

Retrofits for trucks aimed at improving aerodynamic performance and reducing the overall drag coefficient have recently shown great potential [6-8]. Examples of such drag-reducing devices include cab roof and side fairings, tractor and trailer side skirts, trailer-front fairings, vortex generators, and base-flaps. Studies for cab roof and side fairings show 9% to 17% drag reduction percentages on heavy vehicles [9-11]. Moreover, trailer-front fairings provide 7-10% reduction of the baseline drag coefficient as shown by [12]. Base flaps installed on a full-scale tractor-trailer reduce the overall drag coefficient by about 4–5% [10]. Slight modifications on tractors and trailers, such as edge-rounding and rear tapering, can provide further drag reduction [13]. More sophisticated methods such as active boundary-layer control techniques have also been studied on heavy vehicles with promises of significant drag reduction [14-15].

The effect of using retrofits for SUV aerodynamic drag reduction was investigated in [16], where the installation of a boat tail plate resulted in reducing the drag coefficient of a generic SUV by 12.3 %. Other types of drag-reduction techniques were also experimented on SUVs. Lamond et al [17] investigated the use of base bleed on an SUV using computational fluid dynamics. The design introduces air to the rearward low-pressure region by the use of a gas generator, resulting in a reduction of the drag coefficient by 8.2%.

In the present study, a new drag-reducing device is proposed for improving the aerodynamic performance of heavy vehicles. The device consists of lateral guide vanes that are installed near the rear end of the vehicle. The objective of installing the vanes is to guide the air flow into the low-pressure wake region. This would result in a pressure increase in the wake region due to mass addition of the directed air, which in turn would reduce pressure drag and hence the overall aerodynamic drag of the vehicle. Four different cross-sectional types are investigated for the guide vanes namely; flat-plate, NACA 0015, NACA 2412 and NACA 64(3)-218 cross-sections. A numerical parametric study, using computational fluid dynamics, is conducted to investigate the effect of installing the lateral guide vanes on a simplified bus model and a simplified SUV model. The parametric study is concerned with identifying the optimum guide vane cross-section and the optimum angle of attack for maximum drag reduction. In the present study, the commercial CFD package, ANSYS CFX, is used to perform the steady-state RANS simulations.

2. Problem Description

The effects of installing lateral guide vanes on the aerodynamic performance of simplified models for a bus and a sport utility vehicle are investigated in the present study. The bus is simplified using the box model of Tsuei and Savas [18], for which the overall drag coefficient has been experimentally evaluated ($C_D=0.995$). Fig (1) provides a schematic of the box model, with the

exact dimensions being given in table (1). As shown in fig (1), both ends of the rectangular box are flat with sharp corners and edges which would provide a reasonable simulation for a bus or a mini-van [18]. The Reynolds numbers based on the box length and the free stream velocity (120 km/h) is 1×10^6 . As for the SUV model, the Hummer H2 is considered for which the drag coefficient is 0.57 [19]. A simplified model for the Hummer H2 is adopted in the present study and is shown in fig (2). The SUV model is scaled down to fit the same length of the box model ($L=25.4$ cm), in order to maintain a fixed Reynolds number throughout the present study.

Lateral guide vanes are installed as shown in fig (3). The lateral distance $L1$ is taken to be $0.99L$, while the longitudinal distance $L2$ is taken to be $0.55W$. Both distances are fixed for all reported test cases in the present study. For airfoil cross-sections, $L1$ and $L2$ are measured from the leading edge of the airfoil. A three-dimensional view showing the installation of the guide vanes on the box and SUV models is given in fig (4) for further clarification. The orientation of the guide vanes is varied by changing the angle of attack for attaining maximum drag reduction. Four possible cross-sectional shapes are considered for the guide vanes, namely, flat plate, NACA 0015, NACA 2412 and NACA 64(3)-218 cross sections. For the flat plate, the thickness is taken to be 15% of the plate length, which would coincide with the thickness-chord ratio of the NACA 0015 airfoil. A graphical comparison between the different cross-sectional shapes is provided in fig (5).

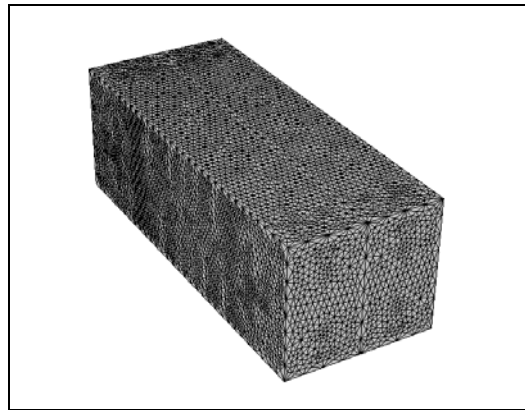


Figure 1. Schematic of the box model

TABLE1: DIMENSIONS OF THE BOX MODEL

Dimensions (cm)	Box Model
Length (L)	25.4
Width (W)	10.2
Height (H)	8.9
Ground clearance (h)	1.3

3. CFD Simulation Setup and Validation

3.1. CFD Simulation Setup

The commercial CFD package, ANSYS CFX, is used in the present study to perform the steady-state RANS simulations. Fig (6) summarizes how the numerical procedure is set up. CFX-Mesh is used to construct the computational unstructured grid which consists of tetrahedral control volumes. Fig (7) shows a cut in the volume mesh at the symmetry plane for the SUV model. The maximum expansion factor for any two adjacent tetrahedral elements is limited to 1.2 to ensure the smoothness of the grid.

CFX-Pre is used for setting up the physical model and the boundary conditions. Two turbulence models are adopted in the present study. The first model is the standard $k-\epsilon$ turbulence model [20] which is implemented together with scalable wall functions [21] to allow for systematic grid refinement without solution deterioration. The second turbulence

model is the SST $k-\omega$ model [22], which is reported to perform better than the $k-\epsilon$ model in the presence of adverse pressure gradients [23]. The working fluid is set to air at 25°C and a uniform velocity profile of 120 km/h is specified at the domain inlet with a 0.5% turbulence intensity level to simulate a low turbulence wind tunnel similar to that in [18]. For the domain outlet, a zero average static pressure boundary condition is applied. No slip conditions are set at the solid walls in order to closely replicate the actual wind tunnel tests of Tsuei and Savas [18]. Moreover, a symmetry boundary condition is specified for the central symmetry plane of the geometry.

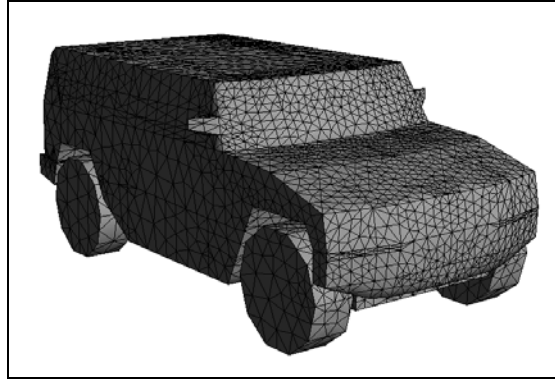


Figure 2. Schematic of the SUV model

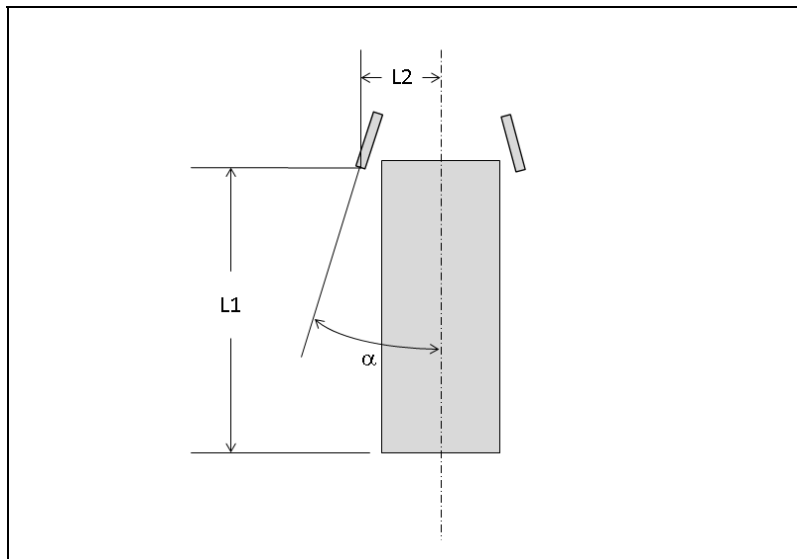
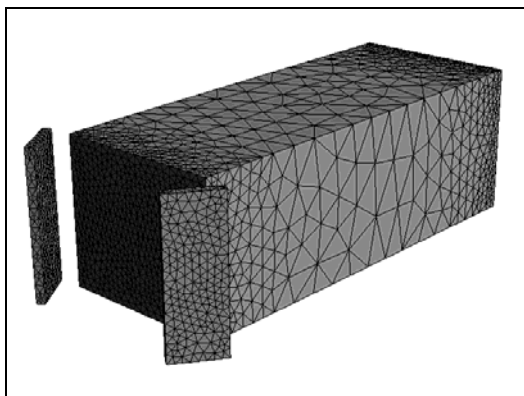
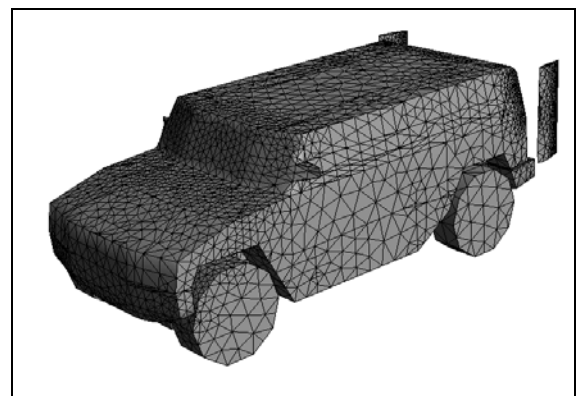


Figure 3. Orientation and dimensions of the installed lateral guide vanes



(a)



(b)

Figure 4. Schematic with lateral guide vanes installed for (a) the box and (b) the SUV models

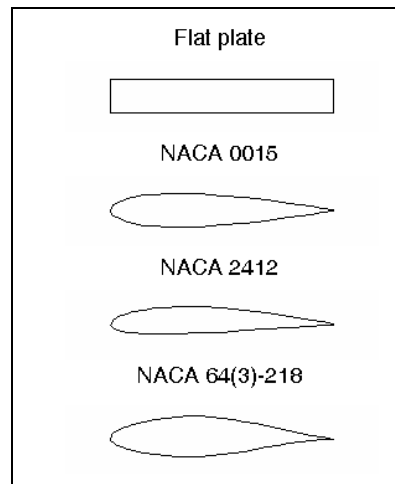


Figure 5. Cross-sectional shapes for the lateral guide-vanes

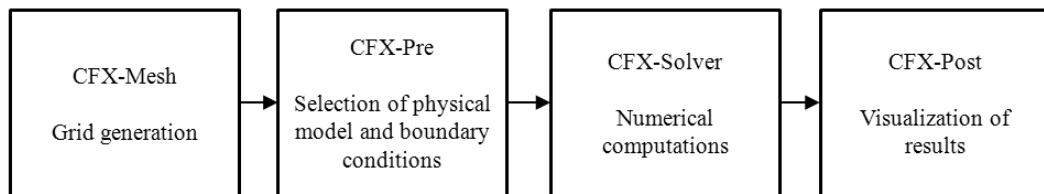


Figure 6. Steps for setting up of the numerical procedure

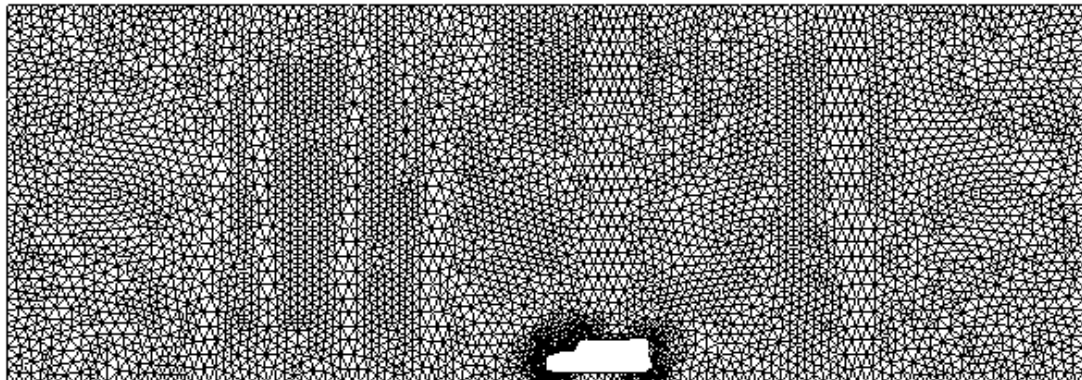


Figure 7. Mesh at the symmetry plane for the SUV model

CFX-Solver performs the numerical computations using a fully implicit finite volume discretization of the RANS equations and a coupled solver. Advection terms are discretized using a high-resolution scheme which is essentially second order accurate. The convergence criterion is set to 10^{-5} for the maximum residuals of all simulation cases reported in the present study. The maximum residuals, within the context of the present study, represent the maximum absolute value of the relative residuals for the mass, momentum, turbulent kinetic energy and turbulent dissipation rate equations. Moreover, the drag coefficient is monitored to ensure that it attains a constant value and is no longer changing with iterations when the convergence criterion is met.

CFX-Post is the 3D graphical post-processor that allows visualization and quantitative post-processing of the results of CFD simulations. Using CFX-Post, the overall drag coefficient for the different models considered in the present study is evaluated from the following equation:

$$C_D = \frac{F_D}{\frac{1}{2}\rho_\infty V_\infty^2 A} \quad (1)$$

where F_D is the computed drag force and A is the frontal area of the vehicle exposed to the oncoming flow. Surface pressure plots can also be generated, where the non-dimensional pressure coefficient is evaluated as follows:

$$C_p = \frac{P - P_\infty}{\frac{1}{2}\rho_\infty V_\infty^2} \quad (2)$$

3.2. Validation of Numerical Procedure

The well-known Ahmed car [24] with a 25° slant angle is simulated first in order to validate the present numerical procedure. Experimental data are available for the Ahmed car in terms of the drag coefficient [25] and the streamwise velocity profiles in the wake [26]. Numerical simulations are performed at a Reynolds number of 7.68×10^5 based on the car height and a bulk velocity of 40 m/s to correspond to the experimental conditions in [26]. Results for the predicted drag coefficient are given in table (2), showing that both the k- ϵ and SST k- ω models provide reasonable predictions for the drag coefficient within 5.3% of the experimental drag coefficient value provided in [25]. Moreover, simulated streamwise velocity profiles along the symmetry plane and in the wake of the body are provided in fig (8) and compared with the experimental velocity profiles provided in [26]. The comparison is done at three streamwise locations, $x=88$, 138 and 188 mm, where $x=0$ corresponds to the rear end of the Ahmed body. As can be seen from fig (8), the numerical simulations are in good agreement with the experimental velocity profiles in the wake.

Further validation of the present procedure is provided through numerical simulations to predict the overall drag coefficient of the box and SUV models with no guide vanes installed. For the box model, the results are summarized in table (3). Both turbulence models predict the drag coefficient for the box with reasonable accuracy, with the SST k- ω model performing relatively better than the k- ϵ model.

Moreover, for the SUV model, the k- ϵ model predicts an overall drag coefficient of 0.593 while the SST k- ω model predicts a value of 0.606. Both values are relatively higher than the commercially documented value for the Hummer H2 [19], $C_D=0.57$, due to the crudeness of the adopted SUV model in the present study which would result in stronger flow separation and hence a higher drag coefficient. These results show that the steady-state RANS approach is capable of predicting the large-scale time-averaged aerodynamic characteristics for the model vehicles considered in the present study with reasonable accuracy.

4. Results and discussion

4.1. Box model results

As can be seen from the present numerical results and previous experimental data [18], the model is characterized by a large drag coefficient value ($C_D \cong 1$) due to strong flow separation from the sharp edges and corners of the box. To improve the aerodynamic efficiency of the model, a drag reducing device, in the form of lateral guide vanes, is installed near the rear end of the box as shown in fig (4). The chord length of the guide vane is taken to be $L/8$, where L represents the length of the box. The main purpose of installing the guide vanes is to direct the

air flow into the low-pressure wake region. This would improve pressure recovery in the wake due to mass addition of the directed air, which in turn would reduce form drag and hence the overall aerodynamic drag of the box.

The effect of varying the angle of attack for the lateral guide vanes on the percentage drag reduction is given in fig (9) for the flat plate and NACA 00015 cross-sections. Significant reduction in the drag coefficient, C_D , (up to 17%) and in the product C_DA (up to 9%) is attained by using the lateral guide vanes on the box model. Note that the percentage reduction in the product C_DA is lower than the percentage reduction in C_D due to the slightly larger frontal area as a result of installing the guide vanes. It should be noted that the percentage reduction in C_DA provides a more accurate measure of the aerodynamic drag reduction in the present study as compared to the percentage reduction in C_D , due to the change in frontal area as a result of installing the guide vanes.

TABLE2: DRAG COEFFICIENT FOR THE AHMED BODY

Study	C_D for box	Deviation from experiment
Experiment [25]	0.338	-
Present - (k- ϵ) model	0.32	5.3%
Present - SST (k- ω) model	0.356	5.3%

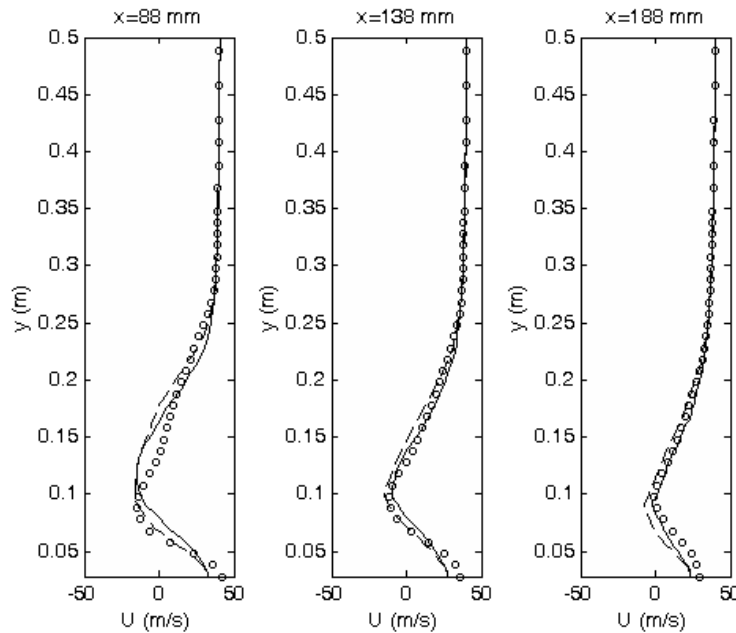


Figure 8: Streamwise velocity profiles along the symmetry plane in the wake of the Ahmed body. Circles represent experiment from [26]. Solid line represents present (k- ϵ) model results. Dashed line represents SST (k- ω) model results.

TABLE3: DRAG COEFFICIENT FOR THE BOX MODEL

Study	C_D for box	Deviation from experiment
Experiment [18]	0.995	-
Present - (k- ϵ) model	0.908	8.74%
Present - SST (k- ω) model	0.915	8.04%

Fig (9) also shows that the performance of the flat plate cross section is inferior to that of the symmetric NACA0015 airfoil cross-section. This should be expected due to the sharp corners of the flat plate that would induce flow separation and hence result in relatively higher

drag as compared to the streamlined airfoil cross section. However it is interesting to note that, even with the use of such an inefficient aerodynamic cross section, drag reduction percentages of up to 13% and 5% are attained for C_D and C_{DA} , respectively. Moreover, from fig (9), it is noticed that maximum drag reduction occurs at small values for the angle of attack. With further increase in the angle of attack, the efficiency of the drag reducing device starts to deteriorate.

To further examine the effect of installing the guide vanes on the pressure recovery in the wake region, the average surface pressure coefficient on the rear surface of the box is evaluated in table (4). With no guide vanes installed, a relatively low average surface pressure coefficient is predicted on the rear surface of the box. When flat plate and NACA 0015 guide vanes are installed at 5° angle of attack, air is directed into the wake region causing a considerable rise in the average surface pressure coefficient value, as can be seen from table (4).

More understanding of the effect of installing the lateral guide vanes on the aerodynamic performance of the box model could be provided through plotting the surface pressure distribution. Fig (10) provide the upper and lower surface pressure distributions for the box at the symmetry plane, with and without installing NACA 0015 guide vanes at 5° angle of attack. In fig (10), the plot starts from the stagnation point on the front side of the box ($x/L=0$) and proceeds over the upper and lower surfaces respectively, terminating with the intersection edge between the surface and the back side of the box ($x/L=1$). As can be seen from figs (10), the installed guide vanes lead to higher pressures on the lower and upper surfaces near the rear end of the box, which indicate improved pressure recovery in the wake region and hence a significantly lower overall drag coefficient.

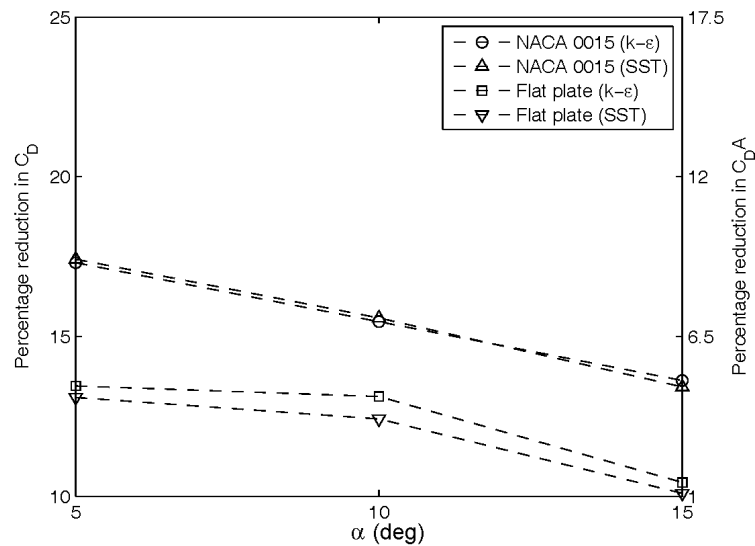


Figure 9: Percentage drag reduction for the box model using lateral guide vanes

TABLE4: AVERAGED C_p ON THE REAR SURFACE OF THE BOX MODEL

Guide vane	α (deg)	C_p	
		k- ϵ	SST k- ω
No guide vane	-	-0.198	-0.216
Flat plate	5	-0.109	-0.126
NACA 0015	5	-0.109	-0.125

4.2. SUV model results

The drag coefficient for the present SUV model is around 0.6, which is a significantly high value. In general, aerodynamic drag can be reduced by increasing the pressure in the SUV base area. Tapering the body sides and roof has a significant effect, but this would reduce the SUV

cargo capacity and the rear passenger headroom. Installation of drag-reducing devices, such as the lateral guide vanes considered in the present study, would improve the aerodynamic performance of the SUV without compromising the cargo room and the rear passenger headroom.

To investigate the effect of installing the guide vanes on the aerodynamic performance of the SUV, two important parameters are identified. These parameters are the vane cross-sectional shape and the angle of attack. The effect of varying these parameters on the percentage drag reduction is given in fig (11) for a chord length of $L/8$. Similar to the trend developed with the box model, installing the lateral guide vanes near the rear end of the SUV model leads to significant reduction in aerodynamic drag. Maximum reduction in the aerodynamic drag coefficient of 18% is predicted with the installation of the guide vanes. Fig (11) also shows that the percentage reduction in the product $C_D A$ is lower than the percentage reduction in C_D due to the larger frontal area as a result of installing the guide vanes. Reduction percentages of up to 10% are predicted for $C_D A$. Again, it should be noted that the percentage reduction in $C_D A$ provides a more accurate measure of the aerodynamic drag reduction in the present study as compared to the percentage reduction in C_D , due to the change in frontal area as a result of installing the guide vanes.

Moreover, and as evident from fig (11), present numerical results indicate that the symmetric NACA 0015 airfoil provides a relatively better performance than the other two airfoils considered.

Table (5) provides further quantitative comparison between the predicted C_D values using the $k-\epsilon$ and SST $k-\omega$ turbulence models for two different chord lengths ($L/8$ and $L/12$). Percentage difference between the predicted C_D values using both turbulence models is within 4% for all reported cases, with the SST $k-\omega$ model consistently predicting a slightly higher C_D value as compared to the $k-\epsilon$ model.

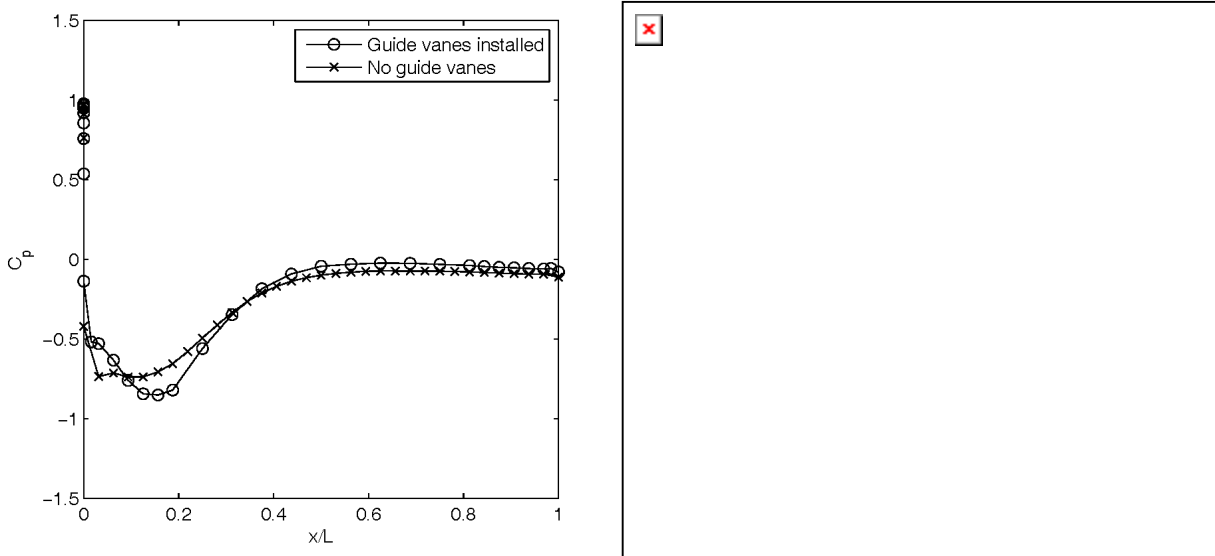


Figure 10. Pressure coefficient distribution on (a) the upper box and (b) the lower box surfaces

5. Grid-independence study

All test cases reported in the present study were simulated on a sequence of increasingly fine meshes in order to ensure grid-independent results. Sample results, using the $k-\epsilon$ turbulence model, are provided in table (6) for the SUV using the NACA 0015 airfoil cross-section for the lateral guide vanes with a 5° angle of attack and an $L/8$ chord length. Table (6) shows that a grid size of 1.4 million cells provides grid-independent results for this test case. In general, for all test cases

reported, grid sizes of around the same order of magnitude, 1.4 million cells, were needed to provide grid-independent results.

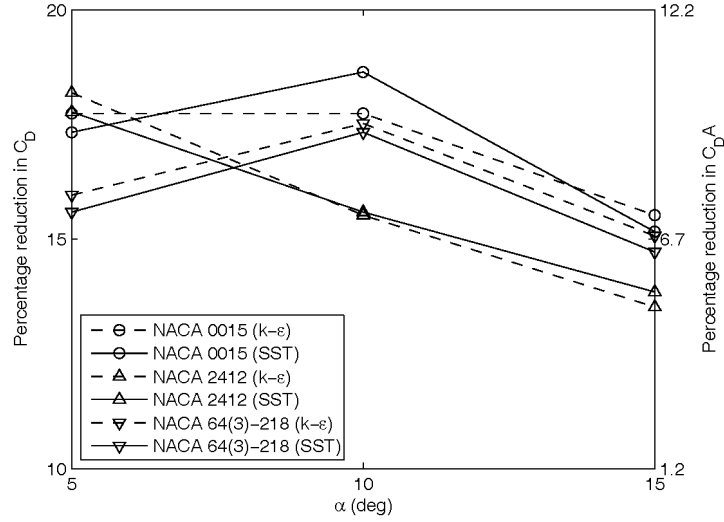


Figure 11. Percentage drag reduction for the SUV using guide vanes of (L/8) chord length

6. Concluding remarks

The effectiveness of a drag reducing device for ground vehicles is numerically investigated in the present study. The device consists of lateral guide vanes that are installed near the rear end of the vehicle. Reduction percentages of up to 18% in the coefficient of drag are reported for simplified bus and SUV models. Moreover, reduction percentages of up to 10% are predicted for C_{DA} . It should be noted that the percentage reduction in C_{DA} provides a more accurate measure of the aerodynamic drag reduction using the present drag reducing device as compared to the percentage reduction in C_D , due to the change in frontal area as a result of installing the guide vanes. Symmetric airfoils, such as NACA 0015, show relatively better performance when used for the guide vanes as compared to flat plate and asymmetric airfoil cross-sections. Reported results in the present study are validated through the use of different turbulence models, performance of grid-independency tests and comparison with experimental results available in the literature.

TABLE5: DRAG COEFFICIENT FOR SUV WITH GUIDE VANES USING DIFFERENT TURBULENCE MODELS

Airfoil	Chord length	α (deg.)	C_D		Percentage difference (%)
			k- ϵ	SST k- ω	
NACA 0015	L/8	5	0.488	0.501	2.66
		10	0.488	0.493	1.02
		15	0.501	0.515	2.79
	L/12	5	0.491	0.501	2.04
		10	0.487	0.501	2.87
		15	0.493	0.512	3.85
NACA 2412	L/8	5	0.485	0.499	2.89
		10	0.501	0.512	2.20
		15	0.513	0.522	1.75
	L/12	5	0.496	0.504	1.61
		10	0.493	0.501	1.62
		15	0.504	0.515	2.18
NACA 64(3)-218	L/8	5	0.499	0.512	2.61
		10	0.489	0.501	2.45
		15	0.504	0.517	2.58
	L/12	5	0.496	0.501	1.01

	10	0.497	0.501	0.80
	15	0.496	0.516	4.03

TABLE6: GRID-INDEPENDENCE STUDY FOR SUV MODEL USING NACA 0015 GUIDE VANE

Grid Size (number of tetrahedra)	Percentage reduction in C_D (%)
880000	16.17
1040000	17.23
1230000	17.63
1400000	17.74

Nomenclature

A:	Frontal area of model vehicle.
C_D :	Aerodynamic drag coefficient.
C_p :	Pressure coefficient.
F_D :	Aerodynamic drag force.
h:	Ground clearance of model vehicle.
H:	Height of model vehicle.
L:	Length of model vehicle.
P_∞ :	Free stream pressure.
V_∞ :	Free stream velocity.
W:	Width of model vehicle.
α :	Angle of attack for lateral guide vanes.
ρ_∞ :	Free stream density.

References

- [1] Wood, R.M. *Impact of Advanced Aerodynamic Technology on Transportation Energy Consumption*. SAE Technical Paper 2004-01-1306. 2004. Washington, DC.
- [2] Salari K, J. Ortega and P. Castellucci. *Computational prediction of aerodynamic forces for a simplified integrated tractor-trailer geometry*. AIAA Paper 2004- 2253. 2004.
- [3] Pointer D. *Evaluation of commercial CFD code capabilities for prediction of heavy vehicle drag coefficients*. AIAA Paper 2004-2254. 2004.
- [4] Maddox S., K. Squires, K.E. Wurtzler, J. Forsythe. *Detached-eddy simulation of the ground transportation system*. The Aerodynamics of Heavy Vehicles: Trucks Buses and Trains, 2004, Vol. 1: p. 89–104.
- [5] Verzicco R., M. Fatica, G. Iaccarino, P. Moin and B. Khalighi. *Large Eddy Simulation of a Road Vehicle with Drag-Reduction Devices*, AIAA Journal 2002, 40(12): p. 2447–55.
- [6] Wong H.Y., R.N. Cox, A. Rajan, *Drag reduction of trailer-tractor configuration by aerodynamic means*, Journal of Wind Engineering and Industrial Aerodynamics 1981, 9(1): p. 101–11.
- [7] Hyams D.G., K. Sreenivas, R. Pankajakshan, D.S. Nichols, W.R. Briley and D.L. Whitfield. *Computational simulation of model and full scale Class 8 trucks with drag reduction devices*, Computers and Fluids 2011, 41(1): p. 27–40.
- [8] Mohamed-Kassim Z and A. Filippone. *Fuel savings on a heavy vehicle via aerodynamic drag reduction*, Transportation Research Part D 2010, 15(5): p. 275–284.
- [9] Drollinger R.A. *Heavy Duty Truck Aerodynamics*. SAE Technical Paper 870001. 1986. Washington, DC.
- [10] Cooper K.R. *Truck Aerodynamics Reborn-Lessons from the Past*. SAE Technical Paper 2003-01-3376. 2003.
- [11] Leuschen J., K.R. Cooper. *Summary of full-scale wind tunnel tests of aerodynamic drag-*

- reducing devices for tractor-trailers*. The Aerodynamics of Heavy Vehicles II: Trucks, Buses, and Trains 2009, Vol. 2: p. 451-62.
- [12] Watkins S., J.W. Saunders and P.H. Hoffman. *Comparison of road and wind tunnel drag reductions for commercial vehicles*. Journal of Wind Engineering and Industrial Aerodynamics 1994, 49(1): p. 411–420.
- [13] Cooper K.R., *The Effect of Front-Edge Rounding and Rear-Edge Shaping on the Aerodynamic Drag of Bluff Vehicles in Ground Proximity*, SAE Technical Paper 850288. 1985. Washington, DC.
- [14] Buckley Jr. F.T., C.H. Marks. *Feasibility of active boundary-layer-control methods for reducing aerodynamic drag on tractor trailer trucks*, Journal of Wind Engineering and Industrial Aerodynamics 1979, 4(2): p. 133–48.
- [15] Krajnovic S., J. Fernandes. *Numerical simulation of the flow around a simplified vehicle model with active flow control*, International Journal of Heat and Fluid Flow 2011, 32(1): p. 192-200.
- [16] Krishnani P.N. and D. Zhou, *CFD Analysis of Drag Reduction for a Generic SUV*, in *Proceedings of 2009 ASME International Mechanical Engineering Congress and Exposition*, 2009, p. 589-598.
- [17] Lamond A.D., J.J. Kennedy and M. Stickland. *An Investigation into Unsteady Base Bleed for Drag Reduction in Bluff Two-Box SUV*, in *Proceedings of 4th European Automotive Simulation Conference*. 2009. Munich.
- [18] Tsuei L. and O. Savas. *Transient aerodynamics of vehicle platoons during in-line oscillations*, Journal of Wind Engineering and Industrial Aerodynamics 2001, 89(13): p. 1085–1111.
- [19] Phenix M. *Scale model Mercedes's fish-inspired; bionic concept takes small-car thinking to new depths*. Popular Science 2005, 267(3): p. 30-30.
- [20] Launder B.E. and D.B. Spalding, *The numerical computation of turbulent flows*. Computer Methods in Applied Mechanics and Engineering 1974, 3(2): p. 269–289.
- [21] Menter F.R. and T. Esch. *Elements of Industrial Heat Transfer Predictions*, in *Proceedings of 16th Brazilian Congress of Mechanical Engineering (COBEM)*. 2001. Brazil.
- [22] Menter F.R. *Two-equation eddy-viscosity turbulence models for engineering applications*, AIAA Journal 1994, 32(8): p. 1598–605.
- [23] El-Behery S.M., M.H. Hamed. *A comparative study of turbulence models performance for separating flow*, Computers and Fluids 2011, 44(1): p. 248-57.
- [24] Ahmed S.R. and G. Ramm. *Some salient features of the time-averaged ground vehicle wake*, SAE Technical Paper 840300. 1984.
- [25] Meile W., G. Brenn, A. Reppenhagen, B. Lechner and A. Fuchs, *Experiments and numerical simulations on the aerodynamics of the Ahmed body*, CFD Letters 2011, 3(1), p. 32-39.
- [26] Lienhart H. and S. Becker, *Flow and Turbulence Structure in the Wake of a Simplified Car Model*, SAE Paper 2003-01-0656. 2003. Detroit.